



## A Facile Microwave-Assisted Synthesis of Sodium Alginate-Coated ZnO and CuO Nanoparticles and their Antimicrobial Effects

S. M. Sathiya<sup>1\*</sup>, B. Prakash<sup>1</sup>, M. A. Jothi Rajan<sup>1</sup>, Gunadhor S. Okram<sup>2</sup>

<sup>1</sup>Department of Physics, Arul Anandar College (Autonomous), Karumathur, Madurai, Tamil Nadu, India

<sup>2</sup>Department of Physics, UGC-DAE Consortium for Scientific Research, University campus, Khandwa Road, Indore, Madhya Pradesh, India

\*Corresponding author: S. M. Sathiya, Department of Physics, Arul Anandar College (Autonomous), Karumathur, Madurai, Tamil Nadu, India, Tel: 9443751487; E-mail: sathiya.martin@gmail.com

**Received:** December 02, 2021, Manuscript No. TSCX-21-47957; **Editor assigned:** December 06, 2021, PreQC No. TSCX-21-47957; **Reviewed:** December 20, 2021, QC No. TSCX-21-47957; **Revised:** February 02, 2022, Manuscript No. TSCX-21-47957 (R); **Published:** February 07, 2022

### Abstract

A facile, green, microwave-assisted co-precipitation technique was used for synthesizing Zinc Oxide (ZnO) and Copper Oxide (CuO) Nanoparticles (NPs) in the presence of a bio-polymer Sodium Alginate (SA) as stabilizer and reducer and the mechanism of the formation of NPs was examined. The analysis of the results showed that there is a strong interaction between the hydroxyl and carboxyl groups of SA with the nanostructured metal oxides. These NPs showed considerable antibacterial activities in both *Pseudomonas aeruginosa* and *Bacillus subtilis*. Strong affinity toward hydroxyl and negatively charged carboxyl groups in SA of the NPs with the cell walls of bacterial strains leads to reduction in the bacterial survival significantly. When compared to Gram-positive, both the NPs had better activity against Gram-negative bacterial cultures. The CuO NPs showed maximum zone of inhibition than ZnO NPs due to its intrinsic microbicidal properties.

**Keywords:** Alginate; Stabilizer; Antibacterial

### Introduction

Nanoparticles (NPs) exhibit novel properties for various applications. Critics and others have however, raised questions about the potential toxicity of such materials on living organisms due to either intentional or unintentional contact with them [1,2]. It is also well-known that the reported results of contact on living organisms of NPs are sometimes conflicting [3,4]. Thus, the development of new material at low toxicity in the preparation of NPs attracts an increasing attention [5]. However, stabilization of the NPs, a key role for productive existence of the NPs without aggregation, is an important issue [6-8]. Naturally available polysaccharides are widely used for this purpose.

**Citation:** Sathiya SM, Prakash B, Rajan MAJ, et al. A Facile Microwave-Assisted Synthesis of Sodium Alginate-Coated ZnO and CuO Nanoparticles and their Antimicrobial Effects. ChemXpress. 2022;14(1):001

© 2022 Trade Science Inc

They include chitosan, oligosaccharide, inulin, soluble starch, and xylan, used in the green preparation of metal oxides as reducing and stabilizing agent. Sodium Alginate (SA), an anionic medicinal bio-polymer and sodium salt of alginic acid, is one such natural polysaccharide with an un-branched copolymer with homopolymeric blocks of  $\alpha$ -1,4-linked- D mannuronic acid (M block) and  $\beta$ -1,4-linked-L-guluronic acid (G block) units arranged in an irregular block-wise pattern of varying proportions of GG, MG and MM blocks [9-13].

Polymer incorporated metal oxide-based NPs have tremendous scope because of their potential applications not only in the bio-medical field but also in various important fields such as environment, energy and information technology. There has been a great deal of interest in making polymer incorporated metal oxide-based NPs because the impregnation of metal oxide into a polymer matrix can introduce novel properties to the NPs. According to Raveendran et. al., glucose was used as the reducing agent and starch as the protecting agent for the preparation of Au, Ag, and Au–Ag nanoparticles by an environmentally benign method in water for biological application [14]. In recent years, metal oxides have been extensively used as antibacterial agents towards many pathogens. Among the various metal oxides, Zinc Oxide (ZnO) and Copper Oxide (CuO) nanocrystalline materials have been extensively studied because of their potential anti-bacterial properties, low toxicity and cost effectiveness. In the synthesis of the NPs, the carboxyl groups of the polymer matrix can electrostatically interact with metal ions and form a complex [15,16].

To the best of our knowledge, the microwave assisted co-precipitation technique for preparing well-dispersed nanocrystalline metal oxide in natural polymeric media has not been reported. Hence, we prepared a simple, rapid and totally green, one-pot approach of nanocrystalline metal oxide (ZnO-CuO) NPs using SA and investigated the antibacterial properties against *Pseudomonas aeruginosa* and *Bacillus subtilis*. These have been done after establishing their stabilization, morphologies, and mechanism of their formation.

## Materials and Methods

All reagents were of analytic quality and were used without additional purification. The solutions were prepared with Double Distilled Water (DDW). Copper (II) chloride dehydrate,  $\text{CuCl}_2 \cdot 2\text{H}_2\text{O}$  (Merk, Mumbai, 99% purity), zinc acetate dehydrate,  $\text{Zn}(\text{CH}_3\text{COO})_2 \cdot 2\text{H}_2\text{O}$  (Merk, Mumbai, 99% purity), Sodium Alginate with Mr ~ 48,000-186,000, (Loba Chemie, Mumbai) and sodium hydroxide [NaOH] procured from Merck, Mumbai (98% purity) were used in this work.

## Synthesis of ZnO and CuO nanoparticles

In a typical synthesis process, 1 g of SA was dissolved in 100 mL DDW under vigorous string. After the complete dissolution of SA, 0.3 M (6.5847 g) of  $\text{Zn}(\text{CH}_3\text{COO})_2 \cdot 2\text{H}_2\text{O}$  was dissolved to the above solution. To adjust the pH to 10 of the solution, NaOH was added drop-wise to the above mixture. As the reaction progresses, the colour of the reaction mixture changed to milky white. After 2 hrs of continuous magnetic stirring, the reaction mixture was kept in the microwave oven (operated with frequency 2.45 GHz and electrical power 800 W) at 110°C for 2 min. The solution as prepared was cooled down to room temperature within a short time interval after the reaction, centrifuged, and washed with DDW to remove the by-products.

Then, the obtained product was dried in an oven at 80°C for 3 hrs, named as ZSA and used for characterization. The same

experimental procedure was followed for the synthesis of CuO NPs (named as CSA), by adding 0.3 M (0.51144 g) of  $\text{CuCl}_2 \cdot 2\text{H}_2\text{O}$  instead of  $\text{Zn}(\text{CH}_3\text{COO})_2 \cdot 2\text{H}_2\text{O}$ .

### Antimicrobial Activity (Well-diffusion Method)

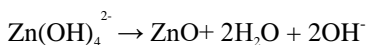
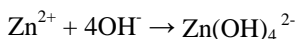
The antibacterial activity of the as prepared samples of ZSA and CSA were done on the microorganisms by well-diffusion method. The samples of various aliquots of 100  $\mu\text{g}/\text{mL}$ , 150  $\mu\text{g}/\text{mL}$ , 200  $\mu\text{g}/\text{mL}$  and stock solution (1  $\text{mg}/\text{mL}$ ) was dispersed in appropriate amount of DDW and constantly stirred until a uniform colloidal suspension was formed. 5.3 g of Muller Hinton agar was dissolved in 100 mL of DDW and kept at  $121^\circ\text{C}$  for about 15-20 minutes for sterilization. Sterilized mixture was poured on the sterilized plates while the temperature of medium was bearable. To assess antimicrobial activity, an appropriate volume of *Pseudomonas aeruginosa* (*P. Aeruginosa*) and *Bacillus subtilis* (*B. Subtilis*) was poured into the nutrient broth medium and equal sizes of wells were created. Three concentration of 100, 150 and 200  $\mu\text{g}/\text{mL}$  of samples were injected into the respective wells along with positive and negative control. For negative control, DDW was used and for positive control, tetracycline (30  $\mu\text{g}/\text{mL}$ ) was used for *P. Aeruginosa*, and cefuroxime (30  $\mu\text{g}/\text{mL}$ ) was used for *B. Subtilis*. The plates were kept overnight for incubation at  $37^\circ\text{C}$ . After the incubation, the zone of inhibition was measured in millimeter (mm). For each concentration, measurements were made in triplicate and their mean value is taken into account for the antibacterial activity of the sample [17].

### Characterization Techniques

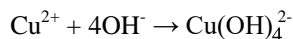
X'Pert Powder PANalytical X-ray diffractometer was used to study X-Ray Diffraction (XRD) patterns. The scan rates were made in the range of  $10-70^\circ$  ( $2\theta$ ) with a step size of 0.02 o and a count time of 2 sec/step. Transmission Electron Microscopy (TEM) analysis was carried out at a 200 kV Tecnai G2 20 microscope, equipped with a  $\text{LaB}_6$  filament and a CCD camera. The sample for IR analysis was prepared by mixing KBr with 10% NP powder by weight and pressing into a vacuum pellet at  $200 \text{ kg cm}^{-2}$  for 1 min. For this purpose, KBr tablets were prepared from the sodium alginate biopolymer, CuO and ZnO NPs, and the FTIR spectrum was obtained in the range  $400-4000 \text{ cm}^{-1}$  with a (Bruker, Germany, Vertex 70) spectrophotometer. Zeta ( $\zeta$ ) potential values were measured using a zeta/nano particle analyser Zetasizer Nano Plus (Micromeritics Instrument corporation, USA). Before zeta potential measurements, all samples were sonicated for 5 minutes.

### Formation Mechanism of ZSA and CSA NC's

Based on the following chemical response, the mechanism of NP formation (CSA and ZSA) likely occurs in the presence of biopolymer sodium alginate is shown in Fig. 1 and Fig. 2. In the first reaction, the metallic ions ( $\text{Zn}^{2+}$  and  $\text{Cu}^{2+}$ ) react with the  $\text{OH}^-$  creating precursor  $\text{Zn}(\text{OH})_4^{2-}$ , by heating together forms a constellation. Contrastingly, alginate poly G-sequences have a tendency to adopt an ordered confirmation through dimerization in the presence of divalent metals, so they act as a precisely regulated environment for the growth of particles of nanometer sizes. Similar reaction occurs in CuO NPs as shown below.



Similarly,



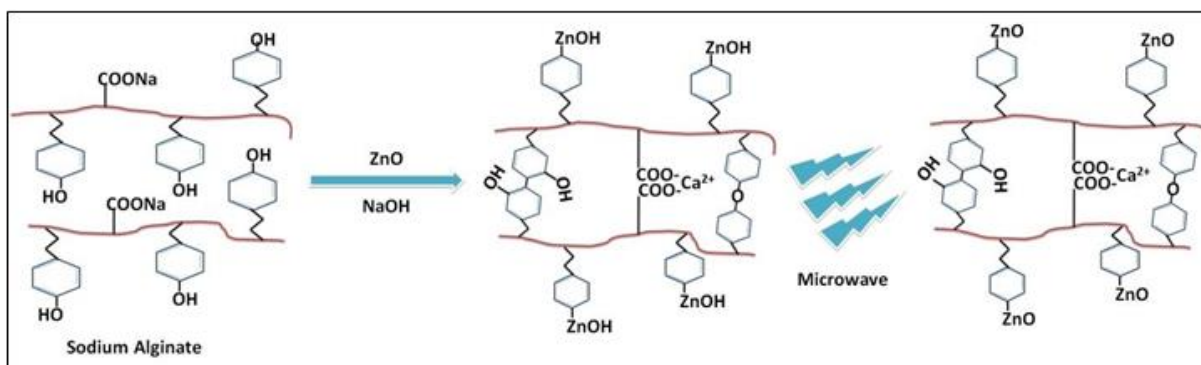


FIG. 1. Schematic representation of the formation mechanism of ZSA nanoparticles.

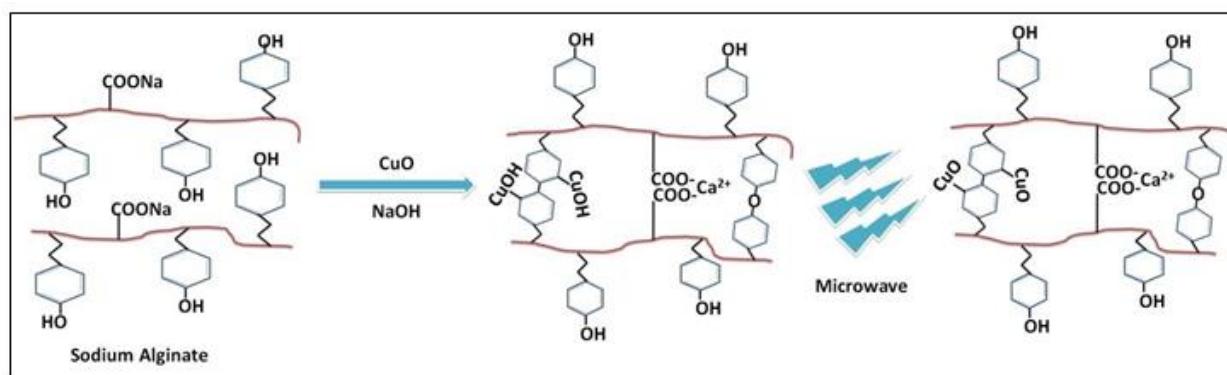


FIG. 2. Schematic representation of the formation mechanism of CSA nanoparticles.

## Results and Discussion

X-Ray Diffraction (XRD) patterns were recorded to study the crystalline nature of the prepared metal oxides. Figure 3 shows the XRD patterns of SA, ZSA and CSA. The peak of SA confirms the semi-crystalline nature with broad reflection peak at  $2\theta=12.7^\circ$ . The diffraction peaks corresponding to ZSA at  $31.6^\circ$ ,  $34.4^\circ$ ,  $36.3^\circ$ ,  $47.5^\circ$ ,  $56.6^\circ$ ,  $62.9^\circ$ ,  $66.4^\circ$ ,  $67.9^\circ$ , and  $69.1^\circ$  are assigned to reflections from the (100), (002), (101), (102), (110), (103) and (200), X-Ray Diffraction (XRD) patterns were recorded to study the crystalline nature of the prepared metal oxides [18]. Figure 3 shows the XRD patterns of SA, ZSA and CSA. The peak of SA confirms the semi-crystalline nature with broad reflection peak at  $2\theta=12.7^\circ$ . The diffraction peaks corresponding to ZSA at  $31.6^\circ$ ,  $34.4^\circ$ ,  $36.3^\circ$ ,  $47.5^\circ$ ,  $56.6^\circ$ ,  $62.9^\circ$ ,  $66.4^\circ$ ,  $67.9^\circ$ , and  $69.1^\circ$  are assigned to reflections from the (100), (002), (101), (102), (110), (103), (200), (112), and (201) planes of the ZnO crystal, respectively, which confirm the crystalline nature of ZnO. They indicate that the obtained ZnO is phase pure wurtzite structure of ZnO (JCPDS card no: 36-1451). The existence of diffraction peaks at  $12.2^\circ$  corresponding to the peaks of SA, clearly shows that the indication of the existence of SA polymer in NPs. The carboxyl and the hydroxyl groups present in the polymer matrix make bonding to the zinc ions. The XRD pattern thus clearly illustrates that there may be an interaction of ZnO nanoparticles with the polymer

(SA) matrix.

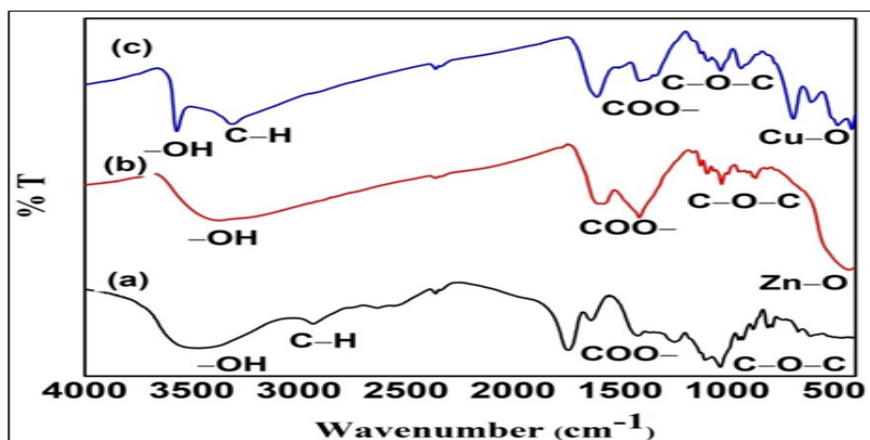


FIG. 3. Schematic representation of the formation mechanism of CSA nanoparticles.

The diffraction peaks of CSA at approximately  $33.9^\circ$ ,  $35.5^\circ$ ,  $38.6^\circ$ ,  $39.8^\circ$ ,  $48.8^\circ$ ,  $53.1^\circ$  and  $58^\circ$  are assigned to reflections from the (002), (-111), (111), (200), (-202), (020) and (202) matching JCPDS card no: 80-0076 confirm the formation of monoclinic structure CuO. The diffraction peaks at  $13.6^\circ$  corresponding to the peaks of SA shows that there is an intercalation of CuO with the polymer matrix. The other crystalline peaks at  $2\theta=16.8^\circ$ ,  $23.8^\circ$ ,  $26.5^\circ$ ,  $35.5^\circ$  and  $61.6^\circ$  are assigned to  $\text{Cu}_2\text{O}$  (JCPDS Card no: 05-0667). The crystallite size calculated using Scherrer's formula is 15.6 nm for ZSA and 10.8 nm for CSA which well-correlate with that obtained from TEM measurement discussed later. The strain, dislocation density, number of crystallite was calculated and is tabulated in Table 1.

It is observed from these tabulated details, the particle size and number of unit cell of the ZSA and CSA affect the dislocation density of the crystal system indirect proportionality. Dislocation density for a given strain increased with decrease in grain size. Moreover, the smaller the size of the grain, the larger the strain to which the cellular network has been well defined [19].

TABLE 1. The structural parameters of ZSA and CSA nanoparticles.

Sample name	Grain size D (nm)	Lattice strain $\epsilon$ (mm)	Dislocation density $\delta=(1/D^2) \times 10^{15}$ (lines/m <sup>2</sup> )	Number of crystallite $N=(t/D^3) \times 10^{20}$
ZSA	15.6	2.288	4.466	30.832
CSA	10.8	5.106	34.76	1089.5

The Figure 4 shows the FTIR spectra of SA, ZSA and CSA. The peaks at around  $3477 \text{ cm}^{-1}$  and  $2935 \text{ cm}^{-1}$  can be attributed to the stretching vibration of -OH and alkyl C-H bands of sodium alginate. The strong peaks noted at  $1742 \text{ cm}^{-1}$  and  $1418 \text{ cm}^{-1}$  are due to the stretching vibration of  $\text{COO}^-$  (carboxylate ion) groups. The absorption band at  $1031 \text{ cm}^{-1}$  corresponds to C-O-C stretching mode from the glucosidic units and the peak at  $878 \text{ cm}^{-1}$  corresponds to Na-O bond vibration. After the incorporation of metal oxides to the polymer matrix, the band of  $\text{COO}^-$  is shifted from  $1742 \text{ cm}^{-1}$  to  $1587 \text{ cm}^{-1}$  in ZSA and

1607  $\text{cm}^{-1}$  in CSA, indicating that the strong physicochemical interaction between the polymer matrix and the metal oxides in the NPs. This also indicates the presence of SA carboxyl and hydroxyl group on the NPs.

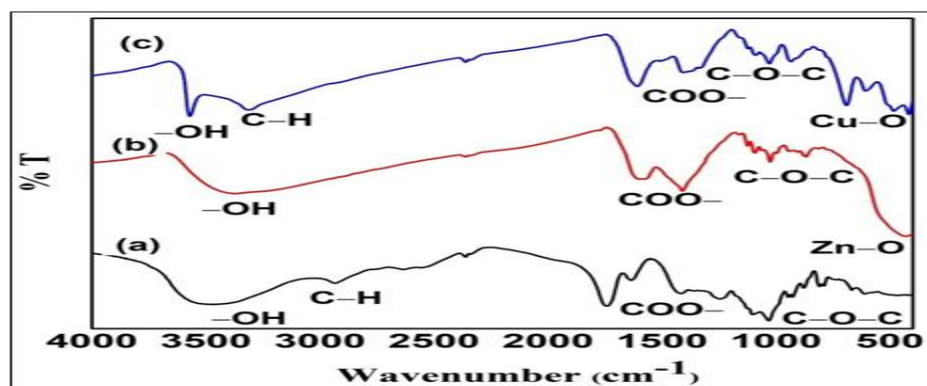


FIG. 4. FTIR spectra of a) sodium alginate b) ZSA and c) CSA NPs.

The particle stability in suspension through electrostatic repulsion between particles can be assessed from zeta potential data as it is an indicator of surface charge. The zeta potential was measured by dispersing 0.1 g of NP's in 10 mL of DDW (Figure 5). The zeta potential of -34 mV in ZSA and -62 mV in CSA indicates the stability of these NPs, and hence indicate good dispersibility of the NPs in DDW when SA is coated as an anionic bio- polymer, which develops a negative charge in the solution. The sample CSA shows more stability than ZSA that may lead to the higher antibacterial activity of the CSA NPs in line with the smaller crystallite size in the former (Table 1).

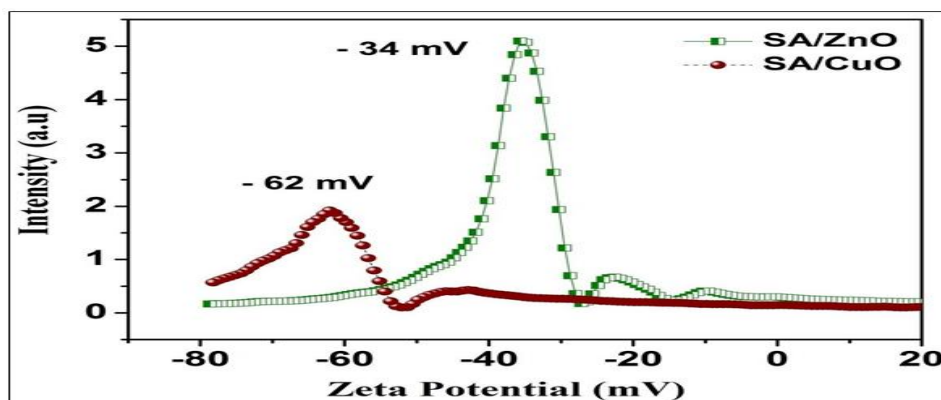


FIG. 5. Zeta potential of ZSA and CSA NPs.

To understand better the effects of the synthesis environment on the shape and size of the NPs, TEM was used (Figure 6(a)). It is evident from TEM micrographs that particles are cubical or spherical shape with a slight elongation at one side and the average size of the NPs is about 16 nm well-comparing that determined from the Scherrer size. The Selected Area Electron Diffraction (SAED) pattern gives a clear image of the polycrystalline nature of the ZSA NPs and the ring patterns are well-matched with the associated (hkl) planes as determined from XRD [20].

Needle like agglomerated CuO nanoparticles are seen in the case of CSA with an average diameter of about 11 nm (Figure 6(b)). As discussed in XRD section, the particle size of the NPs can be controlled by SA polymer. This may reflect the dual role of sodium alginate as stabilizing and reducing agent in DDW. The SAED pattern gives a polycrystalline nature of the CSA NPs and rings well-match with the corresponding (hkl) planes as found in XRD.

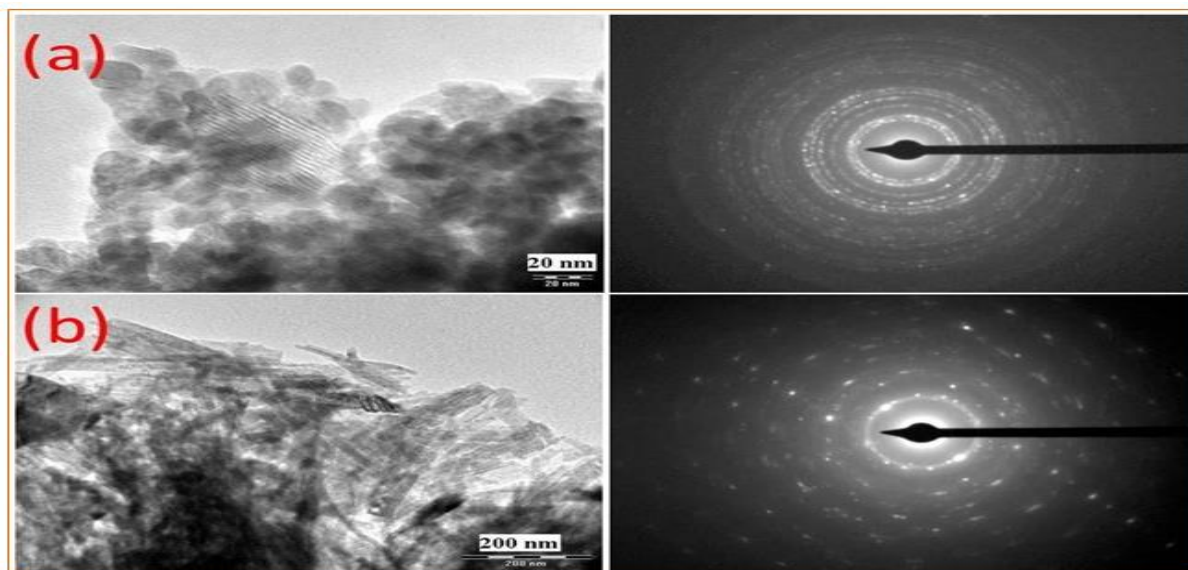


FIG. 6. TEM and SAED patterns of (a) ZSA and (b) CSA NCS.

The effects of NPs on Gram-negative and Gram-positive bacterial strains are tabulated in Table 2. These findings showed that the inhibition zone (ZOI) is maximized and that the effect is more against Gram-negative bacterial strains than Gram-positive bacterial strains. This result may indicate that the ability of the Gram-negative strain against NPs is higher than that of the Gram-positive bacterial strains, and these results are consistent with previous reports. In addition, these findings also suggest that prepared NPs are toxic to Gram-negative and Gram-positive bacteria. The antibacterial properties of the CSA and ZSA NPs against Gram -ve bacteria *Pseudomonas aeruginosa* and Gram +ve bacteria *Bacillus subtilis* showed very interesting results. It is evident from Figure 5, *Pseudomonas aeruginosa* showed significant zone of inhibition than *Bacillus subtilis* in both the NPs [21].

Subsequently released metal ions can bind with DNA molecules and lead disorders of the helical structure by crosslinking into and between nucleic acid strands. Metal ions inside bacterial cells also interfere with biochemical processes and result in death of the bacteria. Compared to ZSA NPs, the CSA NPs showed enhanced antibacterial activity against both the bacterial strains. This result may be dependent due to the reduced size of the CSA NPs, surface morphology, shape of the particle (needle like shape in CSA), and the stability of NPs in the colloidal suspension: CSA NPs are more stable than ZSA NPs as evident from zeta values, in line with earlier reports.

TABLE 2. Antibacterial activity of NPs on Gram-negative and Gram positive bacterial strains at varying

concentrations.

Species		P.C		100 (µg/mL)		150 (µg/mL)		200 (µg/mL)	
		SA/ CuO	SA/ ZnO	SA/ CuO	SA/ ZnO	SA/ CuO	SA/ ZnO	SA/ CuO	SA/ ZnO
		ZOI (mm)	<i>Pseudomonas aeruginosa</i> (-)	28	9	9	6	12	11
	<i>Bacillus subtilis</i> (+)	13	15	-	-	14	-	19	8

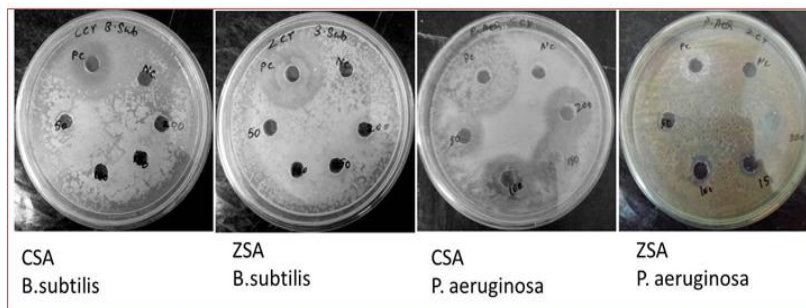


FIG. 7. Antibacterial activity of the samples in Gram-negative and Gram-positive bacterial strains.

The detailed mechanisms of NP bioactivity remain not fully understood. The interaction of NPs over the bacteria could be explained on the basis of five mechanisms is shown in Scheme 3. which were analyzed by several investigations are (1) Indirect effects through changes in the surrounding charge atmosphere, (2) the generation of zeta potential when the NPs are in contact with the cell walls of the bacterial strains, the production of increased levels of reactive oxygen species, mostly hydroxyl radicals and singlet oxygen, (3) the physical blockage by transport channels and damage the cell membrane of bacteria due to loss of membrane potential in bacterial surface (specific binding of the surface of the agent inside the microorganisms), and (4) NPs toxicity of cell membrane by adhesion of particles which further enter into bacterial cell and lyse DNA, protein, mitochondria of the cells and caused bacterial death.

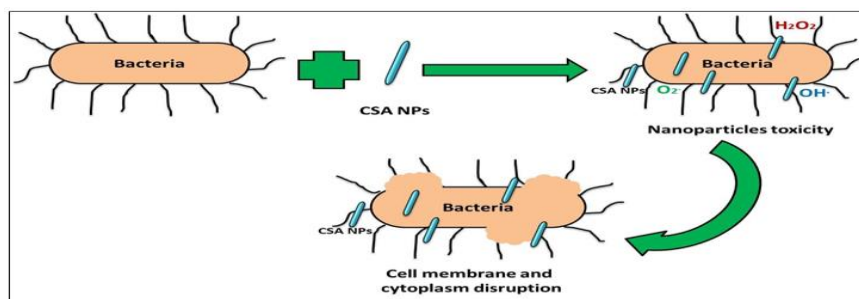


FIG. 8. The mechanisms of the bioactivity of NPs over bacteria.

## Conclusion

The ZnO and CuO NPs were successfully synthesized by microwave-assisted co-precipitation method in the presence of a sodium alginate. There is an indication of strong interaction between the hydroxyl and carboxyl groups present in the polymer matrix and the metal oxides, and these interactions were confirmed by FTIR spectroscopy. The stability of these NPs is well-established from the large zeta potential values. The grain size was calculated from XRD and TEM were around 11 nm in CSA and 16 nm in ZSA. The synthesized NPs had considerable antibacterial activity in both *Pseudomonas aeruginosa* and *Bacillus subtilis*. Compared with Gram-positive, both NP had better activity against Gram-negative bacterial cultures. The CSA NPs show maximum zone of inhibition value than the ZSA NPs. The reduced particle size, increased number of particles, needle like morphology and the increasing stability of the NPs in the colloidal suspension may be the better bacterial activity of the CSA NPs. These findings suggest that prepared NPs could be used in a wide range of biomedical applications because of their attractive structural and antibacterial properties.

## Acknowledgements

The authors gratefully acknowledge UGC DAE CSR, Indore (India) for financial assistance provided to carry out this work through collaborative research project ref. no. CSR-IC/CRS-91/2014-15/597. They also are grateful to UGC DAE CSR, Indore Centre (India) for providing XRD, FTIR, TEM and Zeta Potential facilities. The authors are thankful to the management of Arul Anandar College, Madurai, for providing the facility to carry out this work.

## References

1. Consolo VF, Torres-Nicolini A, Alvarez VA. Mycosynthetized Ag, CuO and ZnO nanoparticles from a promising *Trichoderma harzianum* strain and their antifungal potential against important phytopathogens. *Scientific Rep.* 2020;10:1-9.
2. Sukhanova A, Bozrova S, Sokolov P, et al. Dependence of nanoparticle toxicity on their physical and chemical properties. *Nanoscale Res Lett.* 2018;13:1-21.
3. Sahu SC, Hayes AW. Toxicity of nanomaterials found in human environment: A literature review. *Toxicol Res Appl.* 2017;1:2397847317726352.
4. Ivask A, Juganson K, Bondarenko O, et al. Mechanisms of toxic action of Ag, ZnO and CuO nanoparticles to selected ecotoxicological test organisms and mammalian cells in vitro: A comparative review. *Nanotoxicology.* 2014;8:57-71.
5. Esther J, Sridevi V. Synthesis and characterization of chitosan-stabilized gold nanoparticles through a facile and green approach. *Gold Bull.* 2017;50:1-5.
6. Bae KH, Park M, Do MJ, et al. Chitosan oligosaccharide-stabilized ferrimagnetic iron oxide nanocubes for magnetically modulated cancer hyperthermia. *ACS Nano.* 2012;6:5266-73.
7. Suresh J, Pradheesh G, Alexramani V, et al. Green synthesis and characterization of zinc oxide nanoparticle using insulin plant (*Costus pictus* D. Don) and investigation of its antimicrobial as well as anticancer activities. *Adv Nat Sci: Nanosci Nanotechnol.* 2018;9:015008.
8. Santillán-Urquiza E, Arteaga-Cardona F, Torres-Duarte C, et al. Facilitation of trace metal uptake in cells by inulin coating of metallic nanoparticles. *Royal Soc Open Sci.* 2017;4:170480.
9. Kumar SV, Bafana AP, Pawar P, et al. High conversion synthesis of <10 nm starch-stabilized silver nanoparticles using microwave technology. *Scientific Rep.* 2018;8:1-0.
10. Kolya H, Pal S, Pandey A, et al. Preparation of gold nanoparticles by a novel biodegradable graft copolymer sodium alginate-g-poly (N, N-dimethylacrylamide-co-acrylic acid) with anti-micro bacterial application. *Euro Polymer J.* 2015;66:139-48.
11. Pariy IO, Ivanova AA, Shvartsman VV, et al. Piezoelectric response in hybrid micropillar arrays of poly (vinylidene fluoride) and reduced graphene oxide. *Polymers.* 2019;11:1065.
12. Raveendran P, Fu J, Wallen SL. A simple and "green" method for the synthesis of Au, Ag, and Au-Ag alloy nanoparticles. *Green Chem.* 2006;8:34-8.
13. Sathiya SM, Okram GS, Rajan MJ. Structural, optical and electrical properties of copper oxide nanoparticles prepared

- through microwave assistance. *Adv Mater Proceed.* 2021;2:371-7.
14. Samanta HS, Ray SK. Synthesis, characterization, swelling and drug release behavior of semi-interpenetrating network hydrogels of sodium alginate and polyacrylamide. *Carbohydrate Polymers.* 2014;99:666-78.
  15. Vahidhabanu S, Abideen Idowu A, Karuppasamy D, et al. Microwave initiated facile formation of sepiolite-poly (dimethylsiloxane) nanohybrid for effective removal of congo red dye from aqueous solution. *ACS Sustain Chem Eng.* 2017;5:10361-70.
  16. Cordero-Arias L, Cabanas-Polo S, Goudouri OM, et al. Electrophoretic deposition of ZnO/alginate and ZnO-bioactive glass/alginate composite coatings for antimicrobial applications. *Mater Sci Eng C Mater Biol Appl.* 2015;55:137-44.
  17. Krishna PG, Ananthaswamy PP, Yadavalli T, et al. ZnO nanopellets have selective anticancer activity. *Mater Sci Eng: C.* 2016;62:919-26.
  18. Kumar PV, Kalyani RL, Veerla SC, et al. Biogenic synthesis of stable silver nanoparticles *via Asparagus racemosus* root extract and their antibacterial efficacy towards human and fish bacterial pathogens. *Mater Res Express.* 2019;6:104008.
  19. Azam A, Ahmed AS, Oves M, et al. Antimicrobial activity of metal oxide nanoparticles against Gram-positive and Gram-negative bacteria: A comparative study. *Int J Nanomed.* 2012;7:6003.
  20. Vo NL, Van Nguyen TT, Nguyen T, et al. Antibacterial shoe insole-coated CuO-ZnO nanocomposite synthesized by the sol-gel technique. *J Nanomater.* 2020;2020.
  21. Qiu S, Zhou H, Shen Z, et al. Synthesis, characterization, and comparison of antibacterial effects and elucidating the mechanism of ZnO, CuO and CuZnO nanoparticles supported on mesoporous silica SBA-3. *RSC Adv.* 2020;10:2767-85.